Dalton Transactions

ROYAL SOCIETY OF CHEMISTRY

PAPER

View Article Online
View Journal | View Issue

Cite this: *Dalton Trans.*, 2025, **54**, 16372

A bimetallic Ru(II)–Ru(II) complex as an effective non-small cell lung cancer photosensitizer with potential ferroptosis photoinduction

Kelun Cui,[a] Yuqing Wei,[a] Sufen Si,[b] Qiuyun Chen,[a] Gaoji Wang,[a] Songlin Xue,[a] Yue Wang,*[a] Chunyin Zhu*[a] and Feng Chen*[a]

Received 18th June 2025,
Accepted 16th October 2025

DOI: 10.1039/d5dt01430a

rsc.li/dalton

Three polypyridyl bimetallic photosensitizers of **Ru–Ru**, **Os–Os**, and **Ru–Os** with the general formula of $[(DIP)_4M_2(L\text{-}1)](PF_6)_4$, where DIP is 4,7-diphenyl-1,10-phenanthroline and L-1 is the bridging ligand, were developed and fully characterized. Electronic property study by DFT and TD-DFT calculations indicated a polarized electron distribution tendency and an intra-molecular charge transfer effect. The complex **Ru–Ru** generated high amounts of reactive oxygen species ($^1O_2$ and $O_2^{\bullet-}$), and the $^1O_2$ generation efficiency of **Ru–Ru** was approx. 24 fold (in acetonitrile) and 6.6 fold (in PBS/DMSO (95/5, v/v)) higher than that of $[Ru(bpy)_3]Cl_2$ under low-power blue light exposure. These complexes exhibited moderate to great photocytotoxicity against A549 and MGC-803 cancer cell lines under blue LED light irradiation, and the IC_{50} values of **Ru–Ru** were as low as 2.33 μM (phototherapeutic index (PI) > 21) and 3.10 μM (PI > 16), respectively; while it was relatively less cytotoxic against HaCaT normal cells (**Ru–Ru**, IC_{50} value of 6.10 μM) and almost noncytotoxic in the dark. The cellular singlet oxygen detection in A549 cancer cells was in a concentration-dependent manner. **Ru–Ru** can also induce potent photo-oxidation of NADH (turnover frequency of 462 h^{-1} in PBS) and glutathione in PBS/DMSO (95/5, v/v), interfere with the balance of NADH (41%) and GSH (66%) in A549 cells, and cause accumulated lipid peroxidation, which indicated that such a complex can be a candidate catalytic type I and type II photosensitizer and potentially induce ferroptosis in cancer cells.

1. Introduction

Transition metal complexes with d^6 low-spin metals, in particular of Ru(II) and Os(II), have been intensively studied with regard to their outstanding photophysical, electrochemical, and photo-redox properties.[1,2] In recent decades, considerable efforts have been devoted to developing new polypyridine transition metal complexes as photosensitizers (PSs), concerning the efficiency boost of photon to electron or energy transfer *via* metal–ligand-charge-transfer (MLCT) within the complex.[3] Thus, by fully taking advantage of the photo-quality of the polypyridine complexes, d^6-metal complex based photodynamic therapy has been developed as a prominent complementary strategy to platinum-associated chemotherapy for the treatment of cancers or pathogenic infections,[4] *via* the generation of reactive oxygen species ($O_2^{\bullet-}$ and $^{\bullet}OH$, type I) or singlet oxygen ($^1O_2$, type II). Among those, TLD-1433 represents one of the most successful Ru(II) PSs which is under phase-II clinical trial for non-muscle invasive bladder cancer treatment.[5–7] The potential clinical application has inspired the pertinent design of more functionalized PSs;[8,9] for instance, benefiting from the significant heavy atom effect, Gasser *et al.* reported a series of osmium(II) polypyridyl complexes that showed promising phototoxicity against multicellular tumor spheroids upon near-infrared irradiation at 740 nm.[10] Recently, they have released a new Ru(II) polypyridyl complex ligated with COUPY coumarins that targets hypoxic solid tumors.[11]

Complexes with multitopic-metal centers may exhibit outstanding photo-physical/-chemical properties, *e.g.* photoinduced electron and energy transfer processes, in comparison with the mononuclear analogues.[12–14] Metal centers connected by bridging ligands will display effective electron transfer or an energy coupling effect between each chromophore under light exposure, and any modification of bridging ligands or metals center can promote the electron transfer, leading to unexpected photophysical performance.[15,16] Gou *et al.* developed a self-assembly-induced vibronic decoupling strategy for enhanced $^1O_2$ generation by a homoleptic Ir(III) complex under NIR excitation, while only a trivial amount of $^1O_2$ was produced in the monomeric state.[17] A binuclear Os(II) polypyridyl complex reported by Gao *et al.* showed solely a photothermal (PTT) effect under 808 nm

[a]*School of Chemistry and Chemical Engineering, Jiangsu University, Zhenjiang, China. E-mail: yue.wang@ujs.edu.cn, zhucycn@gmail.com, fengjchen@ujs.edu.cn*
[b]*Northern Light Quality Inspection Technical Service Co., Ltd, Nanjing 210033, China*

irradiation with rare $^1O_2$ generation, while modification of the metal center from homoleptic Os(II)–Os(II) to heterogenous Ru(II)–Os(II) significantly enhanced the $^1O_2$ generation capacity and the PTT effect (Scheme 1).[18,19] Recently, Huang *et al.* have explored a new polypyridyl Ru(II) complex with strong NIR absorption properties, which could induce a notable redox imbalance and energy metabolism perturbation under 700 nm irradiation (Scheme 1).[20] Capitalizing on these compelling investigations, our group have endeavoured to study the photophysical, photo-chemical and biological properties of multinuclear transition metal complexes; in previous research, we have reported a homogeneous dinuclear Os(II) complex based on a symmetrical ligand of ^{t}Bu-DQPP, showing antiproliferative activity towards gastric cancer cells (Scheme 1).[13] In the current work, we have synthesized three bimetallic complexes, **Ru–Ru**, **Ru–Os**, and **Os–Os**, and photo-excited reactive oxygen species generation by these complexes was studied using spectroscopic methods; their antiproliferative activity and the relative catalytic mechanism of action were also studied.

2. Results and discussion

2.1 Synthesis and characterization

Three bimetallic complexes were synthesized in two pathways (Scheme 1); in pathway 1, **Ru-1** was obtained by a reaction of 4-formyl-4′-methyl-2,2′-bipyridine (1 equiv.) and $[Ru(DIP)_2]Cl_2$ (1 equiv.) in DMF;[21] **Ru-2** was constructed *via* a Debus–Radziszewski imidazole synthesis route by reaction of **Ru-1** (1 equiv.) with 1,10-phenanthroline-5,6-dione (1 equiv.) in AcOH under reflux; next, the hetero-bimetallic complex **Ru–Os** was obtained by coordination of **Ru-2** with $[Os(DIP)_2]Cl_2$; in pathway 2, the homoleptic complexes **Ru–Ru** and **Os–Os** were synthesized according to the literature.[13,21] All complexes were fully characterized by $^1H/^{13}C$ NMR, HRMS and elemental analysis (Fig. S1–S19). The octanol/water partition coefficients ($\log P_{O/W}$) were also determined, giving the log *P* values of 1.39 (**Ru–Ru**), 1.33 (**Ru–Os**), and 1.28 (**Os–Os**).

2.2 Spectroscopic study

UV-vis spectra of the three bimetallic complexes were determined in acetonitrile; as shown in Fig. 1a and Table 1, sharp peaks between 300 nm and 350 nm can be assigned to the IL ππ* transitions of the DIP ligand; two adjacent broad peaks at *ca.* 450 and 500 nm of **Os–Os** are attributable to the metal to ligand charge transfer (MLCT) of Os(dπ) toward the chelated ligand L1(π*), and the weak broad band in the range of 600–750 nm, as the elongated tail, is assignable to the spin-forbidden transition of MLCT singlet–triplet transitions for Os(II) PSs, which is typically found in many Os(II) complexes;[12] The broad absorption at around 460 nm for **Ru–Ru** represents the MLCT of Ru(dπ) → DIP and Ru(dπ) → L1 transitions.[22,23] The

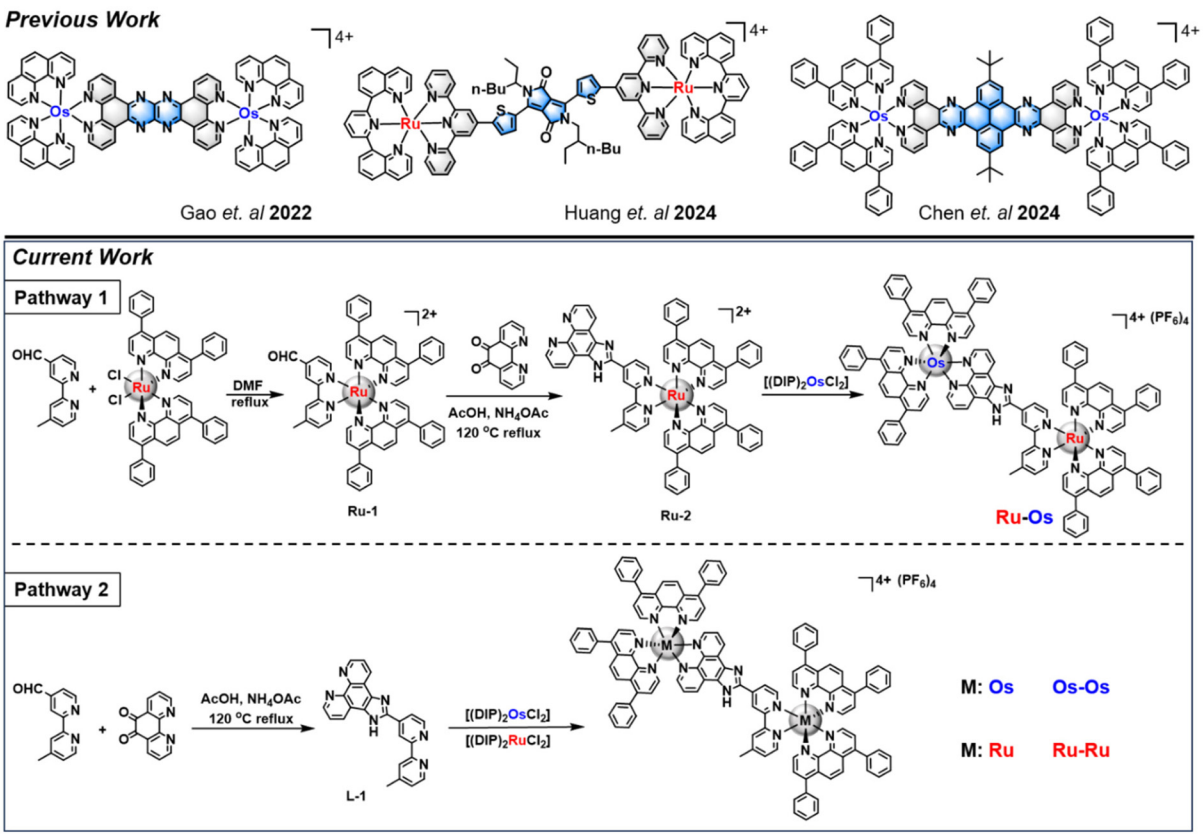

Scheme 1 Previously reported bimetallic complexes and illustrated synthesis routes for the ligand and all complexes.[13,18–20]

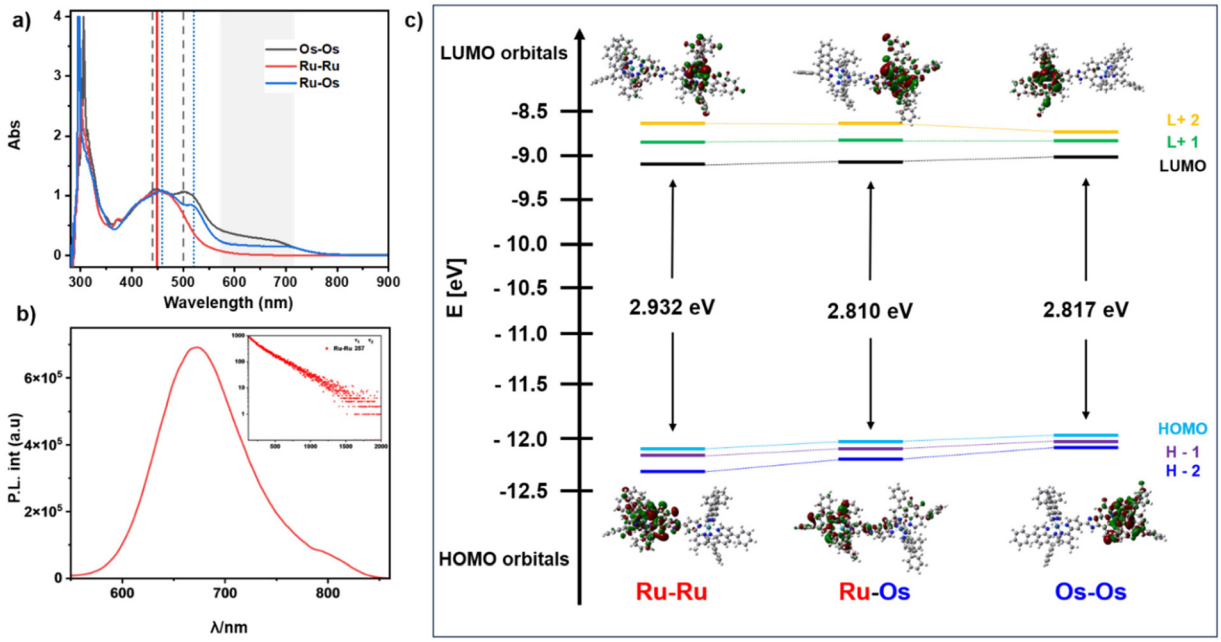

Fig. 1 (a) Absorption spectra of **Ru–Ru**, **Ru–Os**, and **Os–Os** in acetonitrile at room temperature. (b) Emission spectrum of **Ru–Ru** in acetonitrile, inset: photo-luminescence decay of **Ru–Ru**. (c) HOMO and LUMO orbitals of **Ru–Ru**, **Ru–Os**, and **Os–Os**.

adjacent two broad peaks for **Ru–Os** at *ca.* 458 nm and 512 nm showed a bathochromic shift in comparison with those of **Os–Os**, and the broadband tail for **Ru–Os** was assignable to the spin forbidden singlet to triplet transition of Os(dπ) → ligand MLCT transitions.[24]

Emission spectra of bimetallic complexes were recorded in acetonitrile at room temperature. As shown in Fig. 1b, **Ru–Ru** displayed intense emission at *ca.* 670 nm, corresponding well with the Ru(dπ) to DIP (π*) ^{3}MLCT excited state emission, while the ^{3}MLCT emissions for **Ru–Os** and **Os–Os** were significantly quenched by the Os(II) moiety of the complex, and were too weak to be detected in acetonitrile;[22] the emission lifetime of the bimetallic complexes in acetonitrile was decreased in the order of **Ru–Ru** (257 ns) > **Ru–Os** (2.1 ns) > **Os–Os** (1.7 ns) (Fig. 1b and Fig. S20), and the photoluminescence decay of **Ru–Ru** was far longer than that of **Ru–Os** and **Os–Os** ((Table 1).

2.3 DFT and TD-DFT calculations

Electronic properties of **Ru–Ru**, **Ru–Os**, and **Os–Os** were investigated by DFT calculations according to an established method.[25–28] The electronic gaps between the highest occupied molecule orbital (HOMO) and the lowest unoccupied molecule orbital (LUMO) were 2.932 eV (**Ru–Ru**), 2.810 eV (**Ru–Os**), and 2.817 eV (**Os–Os**). As shown in Fig. 1c, all complexes displayed a polarized tendency for electron distribution for the HOMO and LUMO; HOMO electrons of **Ru–Ru** reside almost exclusively on the imidazole-section Ru(II) chromophore, while LUMO electrons reside on the other side; this was in contrast to the HOMO/LUMO distributions of **Os–Os**. The HOMO for **Ru–Os** distributes mainly on the Ru(II) chromophore, and the LUMO resides solely on the Os(II) side. The polarized distribution may predict a light-driven intramolecular charge transfer (ICT) for these complexes.

Next, TD-DFT calculations were also performed to investigate the electron properties (Fig. S21 and S22). The strongest absorption bands observed in all three complexes originate from the S0 → S5 electronic transition. Charge density difference (CDD) analysis reveals that these transitions exhibit pronounced metal-to-ligand charge transfer (MLCT) character, with both constituent metals contributing significantly to the charge transfer process. However, **Ru–Os** additionally displays ligand-to-ligand charge transfer (LLCT) features. In this complex, electron transfer primarily occurs from the ruthenium-containing moiety (involving both the ligand and the Ru

Table 1 UV-vis absorption, luminescence, lifetime data, electronic gaps and turnover frequencies of NADH-oxidation of three complexes

Compound	Absorption[a], λ_{max}[nm] (10^5 ε/M^{-1} cm^{-1})				Em[a] [nm]	τ[a] [ns]	EG [eV]	TOF[b] [h^{-1}]
Ru–Ru	302(1.31)	451(0.54)	373(0.31)		670	257	2.932	462
Ru–Os	295(2.0)	455(0.54)	515(0.42)		377	2.1	2.810	27.9
Os–Os	306(2.0)	458(0.52)	503(0.53)	372(0.30)	390	1.7	2.817	30.6

[a] Data acquired in acetonitrile. [b] Data determined in PBS/DMSO (95/5, v/v).

center) to the osmium-containing moiety. The lowest-energy absorption bands in all complexes arise from the S0 → S1 excitation and retain the MLCT character. In contrast to the S0 → S5 excitation, the MLCT transitions in both homo- and heteronuclear complexes involve charge transfer contributions predominantly from only one metal center.

2.4 ROS generation

2.4.1 Singlet oxygen – $^1O_2$. The ability of singlet oxygen generation by bimetallic complexes **Ru–Ru**, **Ru–Os**, and **Os–Os** was investigated using an indirect method with ABDA as a trapping probe; $[Ru(bpy)_3]Cl_2$ was used as the positive control, and complexes with ABDA in the dark were set as negative control. Initially, $^1O_2$ generation in acetonitrile was determined under blue LED light irradiation (465 nm, Fig. S23) with a molar ratio of bimetallic complex to ABDA of 1 : 6, and **Ru–Ru** exhibited a high reaction rate that can consume ABDA in 10 min, and the bimetallic complexes showed a decrease order of **Ru–Ru** > **Ru–Os** > **Os–Os**; in a shorter period of time (1 min), as shown in Fig. 2a and b, **Ru–Ru** retained the $^1O_2$ generation potency under blue LED light irradiation and can fully oxidize ADBA in 1 min, and the $^1O_2$ production rate of **Ru–Ru** was approx. 24-fold higher than that of $[Ru(bpy)_3]Cl_2$ [10] (Fig. S24). Next, the $^1O_2$ generation under increased molar ratios of **Ru–Ru** to ABDA, *i.e.*, 1 : 30, 1 : 60, and 1 : 150, was determined under blue LED light irradiation; as shown in Fig. S25, ABDA can be fully oxidized at the ratios of 1 : 30 and 1 : 60, and gratifyingly, *ca.* 80% of ABDA was oxidized at a ratio as high as 1 : 150 in 10 min, indicating the potent $^1O_2$ generation capacity of **Ru–Ru**. Aqueous solutions may result in a lower $^1O_2$ generation efficiency due to the quenching effect.[8] The $^1O_2$ generation ability of bimetallic complexes in DMSO/PBS (5/95, v/v) was investigated under blue LED light irradiation (465 nm). Addition of aqueous species reduced the $^1O_2$ generation rate for both **Ru–Os** and **Os–Os**; while it was unexpected to observe that **Ru–Ru** retained the efficiency and entirely oxidized ABDA within 10 min (Fig. S26). In shorter times, with a ratio of complex to ABDA of 1 : 30, ADBA was totally oxidized in *ca.* 6 min (Fig. 2c and d), and the rate for **Ru–Ru** was about 6.6 times higher than that for $[Ru(bpy)_3]Cl_2$ (Fig. S27). When increasing the **Ru–Ru**/ABDA ratio to 1 : 60 and 1 : 150, **Ru–Ru** still induced ABDA oxidation up to 70% and 52%, respectively, in 10 min (Fig. S28). **Ru–Ru** exhibited a highly powerful $^1O_2$ generation ability in both acetonitrile and aqueous solutions, which was much stronger than that of most reported Ru(II) photosensitizers so far.[10,29–31]

Furthermore, the $^1O_2$ generation was also determined under red LED light irradiation (640 nm) using DPBF as a trapping agent. As exhibited in Fig. S29, **Os–Os** and **Ru–Os** displayed a similar tendency and can decompose DPBF in *ca.* 10 min; while encouragingly, **Ru–Ru** also showed a significant efficiency and can totally consume DPBF in *ca.* 20 min, which was much higher than that of $[Ru(bpy)_3]Cl_2$, for which almost no decomposition of DPBF was observed in 20 min.

2.4.2 Superoxide radical ($O_2^{\bullet-}$) generation. The non-fluorescent dihydrorhodamine 123 (DHR 123) can be oxidized to rhodamine 123 ($Rh123^+$, strong green fluorescence) by ROS, and thus has been used as a trapping probe. Initially, the ROS production by **Ru–Ru**, **Ru–Os** and **Os–Os** was investigated using DHR 123 as the probe under blue LED light irradiation (465 nm, Fig. 2e and Fig. S30); the fluorescence signals at *ca.* 526 nm enhanced significantly with blue LED light irradiation; among the complexes, **Ru–Ru** possessed the highest reaction rate and DHR 123 was fully oxidized in *ca.* 5 min, indicating the potency of **Ru–Ru** in the generation of ROS; while a lower-energy light source (red LED light, 640 nm) greatly weakened the generation efficiency for these complexes, where **Ru–Ru** oxidized *ca.* 30% of DHR 123 in 40 min, and less than 10% oxidation was observed for **Ru–Os** and **Os–Os** (Fig. S31). Furthermore, to confirm the $O_2^{\bullet-}$ generation, electron spin resonance (ESR) measurements were performed using 5,5-dimethyl-1-pyrroline-*N*-oxide (DMPO) as the trapping agent. All signal peaks, as shown in Fig. 2f and Fig. S32, in the range of 3480–3540 G were highly assignable to that of DMPO-OOH, indicating the formation of $O_2^{\bullet-}$.[16,32]

All of the above data indicated that **Ru–Ru** is a highly powerful type-I and type-II photosensitizer.

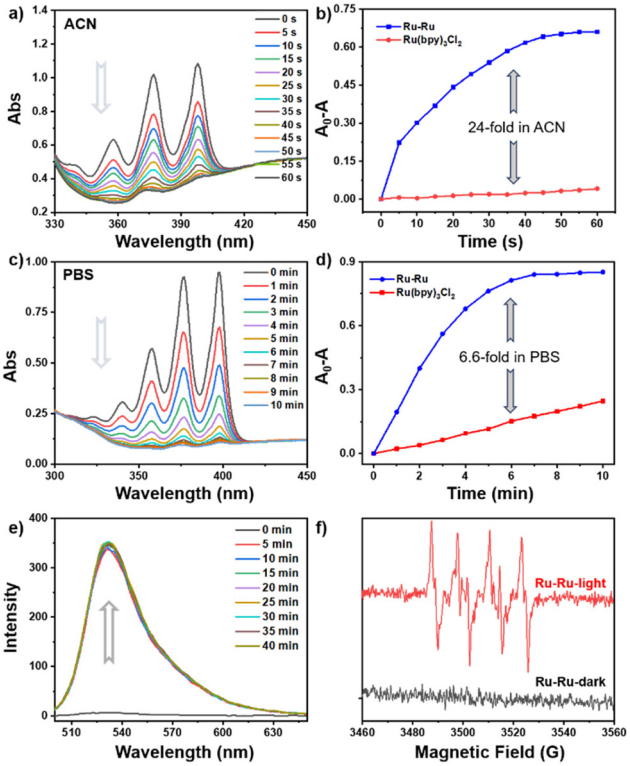

Fig. 2 (a) Absorption spectra of ABDA (60 μM) with **Ru–Ru** (10 μM) in acetonitrile under blue light irradiation (13 mW cm^{-2} for 1 min). (b) Absorbance change at 398 nm of **Ru–Ru** and $[Ru(bpy)_3]Cl_2$. (c) Absorption spectra of ABDA (60 μM) with **Ru–Ru** (2 μM) in PBS/DMSO (95/5, v/v) under blue light irradiation (13 mW cm^{-2} for 10 min). (d) Absorbance change at 398 nm of **Ru–Ru** and $[Ru(bpy)_3]Cl_2$. (e) The change in emission spectra of DHR 123 upon $O_2^{\bullet-}$ generation by **Ru–Ru** (blue, 13 mW cm^{-2} for 40 min, λ_{ex} = 488 nm). (f) The ESR signal of $O_2^{\bullet-}$ trapped by DMPO after blue light irradiation and in the dark.

2.5 *In vitro* antiproliferative activity

Next, the antiproliferative activity of three bimetallic complexes against A549 human non-small cell lung cancer cells, MGC-803 human gastric cancer cells, and HaCaT human normal cells was determined with CCK-8 assay under blue (465 nm) and red (640 nm) LED light irradiation, where 5-ALA was used as positive control (Table S1) and the complex-administered cells without irradiation were set as negative control. As shown in Fig. 3a, 3b and Fig. S33, S34, no cytotoxicity for **Ru–Ru**, **Ru–Os** and **Os–Os** was observed in the dark. Under blue LED light irradiation, **Ru–Ru** induced a significant photocytotoxicity against both A549 and MGC-803 cancer cells, with IC_{50} values as low as *ca.* 2.33 μM and 3.10 μM, respectively, and the phototherapeutic indexes for **Ru–Ru** were >21 and >16 against A549 and MGC-803 cells, respectively. **Ru–Os** and **Os–Os** only showed moderate photo-cytotoxicity against A549 and MGC-803 cancer cell lines. Gratifyingly, **Ru–Ru** displayed lower photocytotoxicity against HaCaT human normal cells, giving an IC_{50} value of 6.10 μM, and the selectivity index values were *ca.* 2.62 and 1.96, indicating a good selectivity of photocytotoxicity between cancer cells and normal cells. However, under blue LED light irradiation, no apparent photocytotoxicity was observed for these complexes against all cell lines (Fig. S35).

2.6 In-cell $^1O_2$ generation, co-localization and cellular uptake

Intracellular $^1O_2$ generation by **Ru–Ru** under blue light irradiation in A549 cancer cells was determined with complex concentrations of 0.2 and 2 μM, using singlet oxygen sensor green (SOSG) as the green fluorescent sensor, and A549 cells with SOSG only were studied as negative control. As evidenced in Fig. 3c, the fluorescence signals of SOSG were observed to be concentration-dependent, and the intensity was significantly improved when co-administered with 2.5 μM and 5 μM **Ru–Ru** under blue LED irradiation, while only weak fluorescence signals were seen in the dark. Furthermore, the potential localization of **Ru–Ru** in cancer cells was investigated by confocal microscopy to study the potential subcellular localization of **Ru–Ru** in A549 cancer cells. MitoTracker Green (MTG, mitochondrial) and DAPI (nucleus) were used as the tracking dyes, and the luminescence of complex **Ru–Ru** appeared as an apparent red signal in A549 cells after 4 h of incubation; however, the red fluorescence signal of **Ru–Ru** showed weak signal overlap with that of MTG (Fig. 3d–g) or DAPI (Fig. S36), suggesting a low tendency of these bimetallic complexes to target mitochondria and the nucleus in cells. The cellular uptake of **Ru–Ru** and **Os–Os** in A549 and MGC-803 cells was studied by inductively coupled plasma mass spectrometry (ICP-MS). Ru contents were found to be *ca.* 180 ng per 10^6 cells in A549 cells and approx. 115.6 ng per 10^6 cells in MGC-803 cells after coincubation, while Os contents in both cells were about 295.4 ng per 10^6 cells(A549) and 271.6 ng per 10^6 cells (MGC-803), and this might indicate a low association with the anticancer activity (Fig. S37).

2.7 NADH oxidation

Nicotinamide adenine dinucleotide (NAD^+) and the reduced form (NADH) play a vital role in biological systems as redox coenzymes, and disrupting the balance of NAD^+/NADH may break off the electron supply in many intracellular redox reactions, thus leading to cell death.[14,33] Initially, the photo-oxidation of NADH by **Ru–Ru**, **Ru–Os**, and **Os–Os** was studied in PBS/DMSO (95/5, v/v) with blue LED light irradiation, and $[Ru(bpy)_3]Cl_2$ was used as a positive control. At a complex/NADH ratio of 1 : 50, **Ru–Ru** showed the highest efficiency in the oxidation reaction and can fully oxidize NADH in 10 min (Fig. S38), and **Ru–Os** and **Os–Os** can oxidize over 90% of NADH in 60 min, and such an NADH oxidation rate was analogous to that of $[Ru(bpy)_3]Cl_2$. Next, the recording time of NADH photo-oxidation by **Ru–Ru** was shortened to 3 min, and gratifyingly, **Ru–Ru** can fully oxidize NADH in 180 s, with a

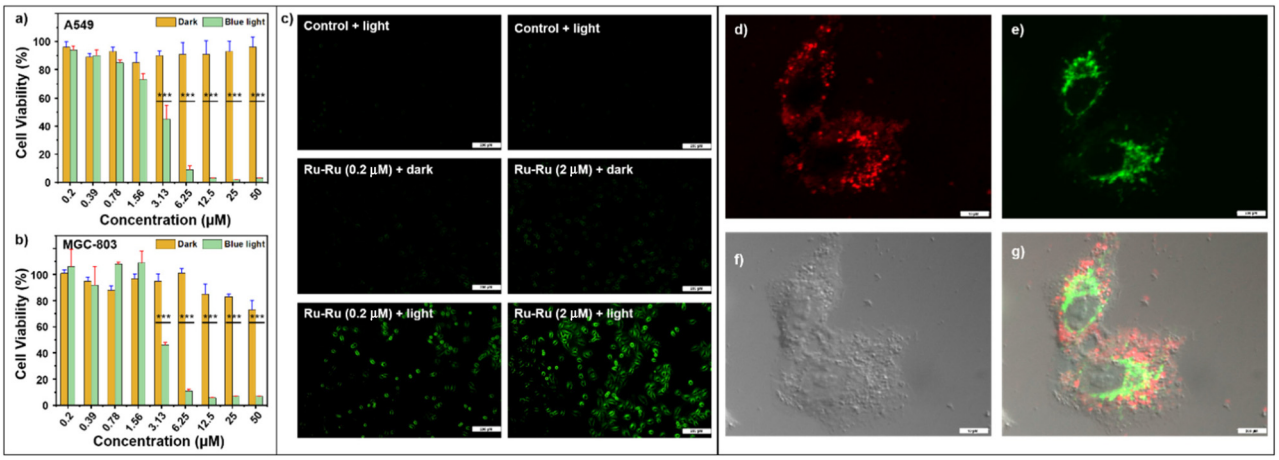

Fig. 3 Cell viability of A549 (a) and MGC-803 (b) cells with various concentrations of **Ru–Ru** under blue light exposure (13 mW cm^{-2} for 1 h) and in the dark. (c) Cellular $^1O_2$ detection by **Ru–Ru** under different conditions in A549 cancer cells with SOSG as the green fluorescent probe. (d) Luminescence of **Ru–Ru** in A549 cells. (e) Mitochondrial localization of MitoTracker Green dye (ex: 488 nm, em: 513–550 nm). (f) Bright field. (g) Merged image.

turnover frequency (TOF) number as high as 462 h^{-1}, which was about 13.6 times higher than that of $[Ru(bpy)_3]Cl_2$ (Fig. 4a). Notably, during the photocatalytic NADH oxidation, the generation of hydrogen peroxide (H_2O_2) was also observed using peroxide detection strips; while no significant H_2O_2 production was observed in the dark (Fig. 4a). Next, the intracellular photo-oxidation of NADH by **Ru–Ru** was investigated in A549 cancer cells, and as shown in Fig. 4b, **Ru–Ru** can induce *ca.* 41% of NADH oxidation under blue light irradiation, indicating a potential NADH oxidation mechanism of action intracellularly.

2.8 Glutathione oxidation and ferroptosis photo-induction

Glutathione (GSH), as an essential tripeptide that can prevent cell damage from ROS, exists ubiquitously in all eukaryotic cells.[34,35] Some of the cell death modes, *e.g.* ferroptosis, are highly GSH dependent.[36] Given the powerful ROS generation by these bimetallic complexes, the photo-activated oxidation of GSH was studied; first, photo-oxidation of GSH by bimetallic complexes with blue LED light exposure was investigated under physical conditions (PBS/DMSO, 95/5, v/v) and was compared with that of $[Ru(bpy)_3]Cl_2$; all complexes can oxidize GSH to GSSG under light exposure, of which **Ru–Ru** displayed a notably higher reaction rate and can induce full photo-oxidation in 5 min (Fig. 4c), which was remarkably higher in comparison with that of $[Ru(bpy)_3]Cl_2$ (*ca.* 40 min, Fig. S39). **Ru–Os** and **Os–Os** showed similar oxidation efficiency and can oxidize GSH to GSSG within 40 min. In a further experiment, intracellular GSH perturbation by **Ru–Ru** under blue LED light irradiation was determined in A549 cancer cells. As shown in Fig. 4d, **Ru–Ru** induced an apparent GSH photo-oxidation that can lower the GSH level by *ca.* 66%, and such a notable reduction of GSH suggests that **Ru–Ru** is capable of disturbing the GSH/GSSG balance in cell.

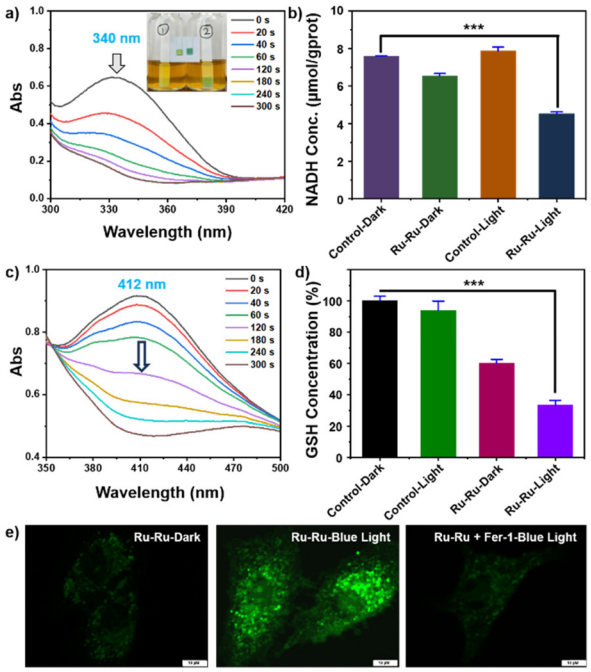

Fig. 4 (a) Photo-oxidation of NADH (100 μM) by **Ru–Ru** (2 μM) in PBS/DMSO (95/5, v/v) with blue light exposure (13 mW cm^{-2} for 5 min), inset: detection of H_2O_2 in the dark (①) and after irradiation (②). (b) Change of NADH levels in A549 cells with different treatments. (c) Photo-oxidation of GSH (100 μM) by **Ru–Ru** (10 μM) in PBS/DMSO (95/5, v/v) with blue light exposure (13 mW cm^{-2} for 5 min). (d) Change of GSH levels in A549 cells with different treatments. (e) The fluorescence of lipid peroxides in A549 cells with different treatments using C11-BODIPY as a trapping probe, ex: 488 nm, em: 520 nm.

Ferroptosis is a new mode of non-apoptotic cell death, with a main feature of inactivation of cellular antioxidant capacity due to the dysfunction of glutathione peroxidase 4 (GPX4, which functions in a GSH-dependent manner).[37,38] Targeting ferroptosis can lead to the peroxidation of accumulated phospholipids containing polyunsaturated fatty acids on the membrane,[32,39] and consumption of GSH may indirectly inhibit the GPX 4 activity, further inducing ferroptosis. Based on the observations above, the potential ferroptosis pathway of **Ru–Ru** was investigated in A549 cancer cells with BODIPY-11 as the trapping dye. As shown in Fig. 4e, the fluorescence of C11-BODIPY in A549 cells treated with **Ru–Ru** was apparently enhanced after blue light exposure, indicating a significant lipid peroxide accumulation; co-administration with the ferroptosis inhibitor ferrostatin-1 (Fer-1) effectively inhibited the fluorescence intensity, which confirmed the ferroptosis photo-induction.

3. Conclusions

In summary, three bimetallic complexes of **Ru–Ru**, **Ru–Os**, and **Os–Os** have been synthesized and fully characterized. The polarized HOMO and LUMO electron distribution indicates the ICT effect for these complexes. Photo-driven $^1O_2$ generation by **Ru–Ru** showed a high reaction rate, which was *ca.* 24-fold (in ACN) and 6.6-fold (in aqueous solution) higher than that of $[Ru(bpy)_3]Cl_2$, and **Ru–Ru** showed potent anticancer activity against A549 and MGC-803 cancer cells under low-power blue light exposure with IC_{50} values as low as 2.33 μM and 3.10 μM, while no cytotoxicity was observed in the dark. Perturbation of NADH and GSH levels both under physical and biological conditions and the photo-induced lipid peroxide accumulation indicate that **Ru–Ru** can be used as a potent type I and II photosensitizer for cancer treatment, with NADH modulation and a potential ferroptosis mechanism.

Author contributions

K. C., C. Z., Q. C., and F. C. designed the project. K. C. and Y.-Q. W. carried out the synthesis and characterisation of ligands and complexes, and determined ROS generation, UV-vis spectra and NADH/GSH photo-oxidation. S. S. and G. W. carried out the antiproliferative cell studies and related

biochemical assays. S. X. and Y. W. carried out the DFT and TD-DFT calculations. All authors contributed to the writing and approved the final version of the paper.

Conflicts of interest

There are no conflicts to declare.

Data availability

The data supporting this article have been included in the supplementary information (SI). Supplementary information: Instruments and materials, synthesis and characterizations, experimental procedures, all supporting table and spectra. Supplementary information is available. See DOI: https://doi.org/10.1039/d5dt01430a.

Acknowledgements

This work was supported by the Natural Science Foundation of China (22207046, 22308132 and 22301108), the Project Startup Foundation of Jiangsu University (4111310026, 5501310019, and 5501310014), the Natural Science Foundation of Jiangsu Province (No. BK20230543), and the College Students' Innovation Project (202410299506X).

A549 human non-small cell lung cancer cells, MGC-803 human gastric cancer cells, and HaCaT human normal cells were provided by Fuheng Biotechnology Co., Ltd (Shanghai, China).

References

1 A. Paul, M. Bar, S. Deb and S. Baitalik, Long-lived trimetallic complexes of Fe(II), Ru(II), and Os(II) based on a heteroditopic bipyridine–terpyridine bridge: Synthesis, photophysics, and electronic energy transfer, *Inorg. Chem.*, 2019, **58**, 10065–10077.

2 Y. Zhang, B.-T. Doan and G. Gasser, Metal-based photosensitizers as inducers of regulated cell death mechanisms, *Chem. Rev.*, 2023, **123**, 10135–10155.

3 S. Deb, A. Sahoo, P. Pal and S. Baitalik, Exploitation of the second coordination sphere to promote significant increase of room-temperature luminescence lifetime and anion sensing in ruthenium–terpyridine complexes, *Inorg. Chem.*, 2021, **60**, 6836–6851.

4 J. Karges, Clinical development of metal complexes as photosensitizers for photodynamic therapy of cancer, *Angew. Chem., Int. Ed.*, 2022, **61**, e202112236.

5 S. Lazic, P. Kaspler, G. Shi, S. Monro, T. Sainuddin, S. Forward, K. Kasimova, R. Hennigar, A. Mandel, S. McFarland and L. Lilge, Novel osmium-based coordination complexes as photosensitizers for panchromatic photodynamic therapy, *Photochem. Photobiol.*, 2017, **93**, 1248–1258.

6 S. Monro, K. L. Colon, H. Yin, J. Roque, P. Konda, S. Gujar, R. P. Thummel, L. Lilge, C. G. Cameron and S. A. McFarland, Transition metal complexes and photodynamic therapy from a tumor-centered approach: Challenges, opportunities, and highlights from the development of TLD1433, *Chem. Rev.*, 2019, **119**, 797–828.

7 J. A. Roque III, H. D. Cole, P. C. Barrett, L. M. Lifshits, R. O. Hodges, S. Kim, G. Deep, A. Francés-Monerris, M. E. Alberto, C. G. Cameron and S. A. McFarland, Intraligand excited states turn a ruthenium oligothiophene complex into a light-triggered ubertoxin with anticancer effects in extreme hypoxia, *J. Am. Chem. Soc.*, 2022, **144**, 8317–8336.

8 Y.-L. Zeng, L.-Y. Liu, T.-Z. Ma, Y. Liu, B. Liu, W. Liu, Q.-H. Shen, C. Wu and Z.-W. Mao, Iridium(III) photosensitizers induce simultaneous pyroptosis and ferroptosis for multi-network synergistic tumor immunotherapy, *Angew. Chem., Int. Ed.*, 2024, **63**, e202410803.

9 Z. Zhao, X. Tao, Y. Xie, Q. Lai, W. Lin, K. Lu, J. Wang, W. Xia and Z.-W. Mao, In situ prodrug activation by an affibody-ruthenium catalyst hybrid for HER2-targeted chemotherapy, *Angew. Chem., Int. Ed.*, 2022, **61**, e202202855.

10 A. Mani, T. Feng, A. Gandioso, R. Vinck, A. Notaro, L. Gourdon, P. Burckel, B. Saubaméa, O. Blacque, K. Cariou, J.-E. Belgaied, H. Chao and G. Gasser, Structurally simple osmium(II) polypyridyl complexes as photosensitizers for photodynamic therapy in the near infrared, *Angew. Chem., Int. Ed.*, 2023, **62**, e202218347.

11 D. Abad-Montero, A. Gandioso, E. Izquierdo-García, S. Chumillas, A. Rovira, M. Bosch, M. Jordà-Redondo, D. Castaño, J. Bonelli, V. V. Novikov, A. Deyà, J. L. Hernández, J. Galino, M. E. Alberto, A. Francés-Monerris, S. Nonell, G. Gasser and V. Marchán, Ruthenium (II) polypyridyl complexes containing COUBPY ligands as potent photosensitizers for the efficient phototherapy of hypoxic tumors, *J. Am. Chem. Soc.*, 2025, **147**, 7360–7376.

12 F. Chen, K. Cui, S. Si, Y. Liu, S. Xue, G. Wang, X. Liang, C. Zhu and Q.-Y. Chen, Polypyridyl Os(II) complexes as efficient human non-small cell lung cancer photosensitizers with enhanced singlet oxygen generation *via* the fused π-ring elongation, *Inorg. Chim. Acta*, 2025, **578**, 122537.

13 Y. Lu and F. Chen, Synthesis and spectroscopic study of a homogenous bimetallic Os(II) complex as a new gastric cancer photosensitizer, *Chem. – Eur. J.*, 2024, e202402861.

14 A. Mandal, V. Singh, S. Peters, A. A. Mandal, T. Sadhukhan, B. Koch and S. Banerjee, Ferrocene conjugated Os(II) complex for photo-catalytic cancer therapy of triple-negative breast cancer cells, *Dalton Trans.*, 2025, **54**, 6785–6789.

15 H.-J. Yin, S. Yu, Y. Yang, C. He and F. Cheng, Ru(II)–Ru(II) and Ru(II)–Os(II) homo-/heterodinuclear complexes and Ru_3(II)–Ru(II) homotetranuclear complexes based on heteroditopic bridging ligands: Synthesis, photophysics, and effective energy transfer, *Inorg. Chem.*, 2024, **63**, 621–634.

16 M. Zheng, X. Lin, K. Xiong, X. Zhang, Y. Chen, L. Ji and H. Chao, A hetero-bimetallic Ru(II)-Ir(III) photosensitizer for effective cancer photodynamic therapy under hypoxia, *Chem. Commun.*, 2024, **60**, 2776–2779.
17 J. Zhao, Y. Gao, R. Huang, C. Chi, Y. Sun, G. Xu, X.-H. Xia and S. Gou, Design of near-infrared-triggered metallo-photosensitizers via a self-assembly-induced vibronic decoupling strategy, *J. Am. Chem. Soc.*, 2023, **145**, 11633–11642.
18 M.-F. Wang, Y.-A. Deng, Q.-F. Li, S.-J. Tang, R. Yang, R.-Y. Zhao, F.-D. Liu, X. Ren, D. Zhang and F. Gao, Dinuclear osmium complexes as mitochondrion-targeting antitumor photothermal agents *in vivo*, *Chem. Commun.*, 2022, **58**, 12676–12679.
19 Y.-A. Deng, S.-J. Tang, M.-F. Wang, X. Ren, X.-L. Li, L.-Z. Zeng, D.-N. Ren, M.-R. Wang, W.-L. Xiao, Z.-Y. Cai, D. Zhang, H. Zhang and F. Gao, Heterometallic ruthenium-osmium complexes: dual photodynamic and photothermal therapy for melanoma and drug-resistant lung tumour in vivo, *Inorg. Chem. Front.*, 2023, **10**, 4552–4561.
20 L. Wei, R. Kushwaha, T. Sadhukhan, H. Wu, A. Dao, Z. Zhang, H. Zhu, Q. Gong, J. Ru, C. Liang, P. Zhang, S. Banerjee and H. Huang, Dinuclear tridentate Ru(II) complex with strong near-infrared light-triggered anticancer activity, *J. Med. Chem.*, 2024, **67**, 11125–11137.
21 F. Cheng, J. Chen, N. Tang, F. Wang and P. Liu, Preparation, photophysical, and electrochemical properties of two polynuclear Ru(II) polypyridyl complexes containing imidazole-based ligands, *Transition Met. Chem.*, 2012, **37**, 721–726.
22 E. C. Constable, E. Figgemeier, C. E. Housecroft, J. Olsson and Y. C. Zimmermann, Electrochemical probing of ground state electronic interactions in polynuclear complexes of a new heteroditopic ligand, *Dalton Trans.*, 2004, 1918–1927.
23 W. Dai, S. Yu, C. Kong, D. Zhao, C. He, Z. Liu, J. Dong, J.-J. Liu and F. Cheng, Effect of electronic structure of energy transfer in bimetallic Ru(ii)/Os(ii) complexes, *Dalton Trans.*, 2023, **52**, 990–999.
24 Z. N. Liu, C. X. He, H. J. Yin, S. W. Yu, J. B. Xu, J. W. Dong, Y. Liu, S. B. Xia and F. X. Cheng, Novel Ru(II)/Os(II)-exchange homo- and heterometallic polypyridyl complexes with effective energy transfer, *Eur. J. Inorg. Chem.*, 2021, 482–491.
25 S. Xue, X. Lv, N. Liu, Q. Zhang, H. Lei, R. Cao and F. Qiu, Electrocatalytic hydrogen evolution of bent bis(dipyrrin) Ni(II) complexes, *Inorg. Chem.*, 2023, **62**(4), 1679–1685.
26 J. Wu, X. Lv, Z. Xue, Y. Wang, F. Qiu and S. Xue, Metal ions control configuration and $^1O_2$ generation capacity of hexaphyrin(2.1.2.1.2.1) with embedded benzene, *Dalton Trans.*, 2025, **54**, 5255–5258.
27 S. Xue, Y. Dong, T. Jiang, J. Wu, Y. Wei, L. Qian, X. Zhao, T. Zhang, F. Qiu and Q. Zuo, Modulation of electrocatalytic overall water splitting performance by β, β′-functionalization of Ni(II) porphyrins, *Inorg. Chem.*, 2025, **64**, 6912–6918.
28 T. Jiang, Y. Hu, S. Liang, F. Qiu, H. Huang, M. Zhou and S. Xue, Ferrocene unit substitution in nickel(II) porphyrin (2.1.2.1) induces an extremely low oxygen evolution reaction overpotential, *Dalton Trans.*, 2025, **54**, 8580–8585.
29 F. M. Wei, S. Kuang, T. W. Rees, X. X. Liao, J. P. Liu, D. Q. Luo, J. Q. Wang, X. T. Zhang, L. N. Ji and H. Chao, Ruthenium(II) complexes coordinated to graphitic carbon nitride: Oxygen self-sufficient photosensitizers which produce multiple ROS for photodynamic therapy in hypoxia, *Biomaterials*, 2021, **276**, 121064.
30 S. Monro, K. L. Colón, H. M. Yin, J. Roque, P. Konda, S. Gujar, R. P. Thummel, L. Lilge, C. G. Cameron and S. A. McFarland, Transition Metal Complexes and Photodynamic Therapy from a Tumor-Centered Approach: Challenges, Opportunities, and Highlights from the Development of TLD1433, *Chem. Rev.*, 2019, **119**, 797.
31 X. Z. Zhao, J. P. Liu, J. L. Fan, H. Chao and X. J. Peng, Recent progress in photosensitizers for overcoming the challenges of photodynamic therapy: from molecular design to application, *Chem. Soc. Rev.*, 2021, **50**, 4185.
32 N. Lu, Z. Deng, J. Gao, C. Liang, H. Xia and P. Zhang, An osmium-peroxo complex for photoactive therapy of hypoxic tumors, *Nat. Commun.*, 2022, **13**, 2245.
33 F. Chen, J. J. Soldevila-Barreda, I. Romero-Canelón, J. P. C. Coverdale, J.-I. Song, G. J. Clarkson, J. Kasparkova, A. Habtemariam, V. Brabec, J. A. Wolny, V. Schünemann and P. J. Sadler, Effect of sulfonamido ethylenediamine substituents in RuII arene anticancer catalysts on transfer hydrogenation of coenzyme NAD^+ by formate, *Dalton Trans.*, 2018, **47**, 7178–7189.
34 A. T. Dharmaraja, Role of reactive oxygen species (ROS) in therapeutics and drug resistance in cancer and bacteria, *J. Med. Chem.*, 2017, **60**, 3221–3240.
35 F. Chen, I. Romero-Canelón, A. Habtemariam, J.-I. Song, S. Banerjee, G. J. Clarkson, L. Song, I. Prokes and P. J. Sadler, Effect of cysteine thiols on the catalytic and anticancer activity of Ru(II) sulfonylethylene diamine complexes, *Dalton Trans.*, 2022, **51**, 4447–4457.
36 X. Wang, F. Chen, J. Zhang, J. Sun, X. Zhao, Y. Zhu, W. Wei, J. Zhao and Z. Guo, A ferroptosis-inducing iridium(III) complex, *Sci. China: Chem.*, 2020, **63**, 65–72.
37 S. J. Dixon, K. M. Lemberg, M. R. Lamprecht, R. Skouta, E. M. Zaitsev, C. E. Gleason, D. N. Patel, A. J. Bauer, A. M. Cantley, W. S. Yang, B. Morrison, 3rd and B. R. Stockwell, Ferroptosis: An iron-dependent form of nonapoptotic cell death, *Cell*, 2012, **149**, 1060–1072.
38 X. Zhao, X. Wang, W. Zhang, T. Tian, J. Zhang, J. Wang, W. Wei, Z. Guo, J. Zhao and X. Wang, A ferroptosis-inducing arsenene-iridium nanoplatform for synergistic immunotherapy in pancreatic cancer, *Angew. Chem., Int. Ed.*, 2024, **63**, e202400829.
39 W. S. Yang, R. SriRamaratnam, M. E. Welsch, K. Shimada, R. Skouta, V. S. Viswanathan, J. H. Cheah, P. A. Clemons, A. F. Shamji, C. B. Clish, L. M. Brown, A. W. Girotti, V. W. Cornish, S. L. Schreiber and B. R. Stockwell, Regulation of ferroptotic cancer cell death by GPX4, *Cell*, 2014, **156**, 317–331.